

Wideband physical layer cognitive radio using photonic blind source separation

Weipeng Zhang^{1*}, Thomas Ferreira de Lima¹, Chaoran Huang², Eric Blow¹, Simon Bilodeau¹, Aashu Jha¹, Bhavin J. Shastri³ and Paul Prucnal¹

^{1*}Department of Electrical and Computer Engineering, Princeton University, Princeton, 08540, New Jersey, USA.

²Department of Electronic Engineering, The Chinese University of Hong Kong, Hong Kong, Postcode, China.

³Department of Physics, Engineering Physics and Astronomy, Kingston, K7L 3N6, Ontario, Canada.

*Corresponding author(s). E-mail(s): weipengz@princeton.edu;
Contributing authors: tlima@princeton.edu;
crhuang@ee.cuhk.edu.hk; ecb10@princeton.edu;
sbilodeau@princeton.edu ; aashuj@princeton.edu;
bhavin.shastri@queensu.ca; prucnal@princeton.edu;

Abstract

The expansion of communication transmissions incurs increasingly severe crosstalk and interference, and a physical layer cognitive method, called blind source separation (BSS), can effectively address these issues. The BSS requires minimal prior knowledge in recovering signals from their mixtures, showing obliviousness of carrier frequency, signal formats, and channel conditions. However, previous electronic implemented BSS did not fulfill this agility due to the inherently narrow bandwidth of radio-frequency (RF) components, the high energy consumption of the digital signal processor (DSP), and their shared weaknesses in scalability. Here, we report a photonic BSS approach that inherits the merits of optical devices that can fully entitle the advantageous “blindness” feature. Using a microring weightbank built on a photonic chip, besides energy-efficient tuning and WDM-compatible scalability, we demonstrate a broad bandwidth across 13.8 GHz, which covers many standard frequency bands. Our setup also has high accuracy (9-bit) in performing the

signal demixing thanks to a recently developed dithering control method, resulting in higher separability even for the ill-conditioned mixtures.

Keywords: Silicon Photonics, Microwave Photonics, Blind Source Separation

1 Introduction

The limited bandwidth of conventional RF equipment has brought increasing pressure as emerging wireless telecommunication services [1, 2] are squeezed into the otherwise limited frequency band resources, witnessing the growth of information density. Thus, many strategies are deployed to maximize the spectrum utilization [3], such as the multi-input-multi-output (MIMO) scheme [4, 5] enhances the data-carrying capacity by space-division multiplexing [6]. However, the inevitable downsides incurred are degraded signal quality due to severe crosstalk between tightly packed spatial channels and the negative impacts on the scientific community by RF interference. Science services, such as weather prediction and radio astronomy, must sensitively detect noise-like signals at frequencies dictated by physical phenomena (shown in Fig. 1c), and the raised vulnerability cannot be avoided by arbitrarily altering the frequency. One mitigation is the active radio access sharing through cognitive radio, which allocates the secondary users with access to the unlicensed bands in the absence of its primary users. Still, it relies on a complicated radio-signal identification mechanism [7] and is vulnerable to privacy breaches [8].

A physical layer cognitive technique called the Blind source separation (BSS) [9] can extract unknown signals (e.g., a signal of interest and an interferer) from their mixtures with minimal prior assumptions. This unique “blindness” allows agility in recovering sources with arbitrary characteristics, such as frequency, modulation type, and power ratio. Yet, this advantage cannot be valid without BSS being performed across a wide frequency range, which is unfortunately not uncommon for the electronically implemented BSS setups due to the limited bandwidth of RF technology. Given that the spectrum of ultra-wideband (UWB) signals [10] covers across up to 7.5 GHz and that of Wi-Fi signals has expanded from 2.4 GHz (802.11) to 6 GHz (802.11ax), to have such broadband coverages is challenging via a single RF setup, as indicated in Fig. 1b and c. Otherwise, using multiple subsystems designed for distinct frequencies can expand the covered bandwidth [11], but at the cost of unavoidable bulkiness and high energy consumption that increases proportionally to the frequency.

By upconverting to frequencies of hundreds of terahertz, the photonic signal processors are very capable of dealing with broadband information [12–14], which regard even GHz signals as narrowband and have low energy consumption that does not scale with the signal frequency. A promising on-chip processor is the microring resonator (MRR) weightbank [15], which provides

energy-efficient tuning and good scalability through the wavelength-division-multiplexing (WDM). Thus, an MRR weightbank-realized RF frontend (as depicted in Fig. 1a) can share the workload of signal processing with the DSP backend and enhances the performance in many aspects. Nevertheless, the MRR bears a weakness in that their high sensitivity in tuning incurs vulnerability to environmental fluctuations and thermal crosstalk between adjacent MRRs. As a result, the tuning accuracy was constrained to around 7 bits [16], and the related BSS performance was barricaded, reflected in low separabilities (the percentage of the signal of interest contained in the recovered signal) and large unwanted signal residuals [17]. It is fortunate that the recently developed dithering control method [18] could release this performance bottleneck via an improved 9-bit accuracy.

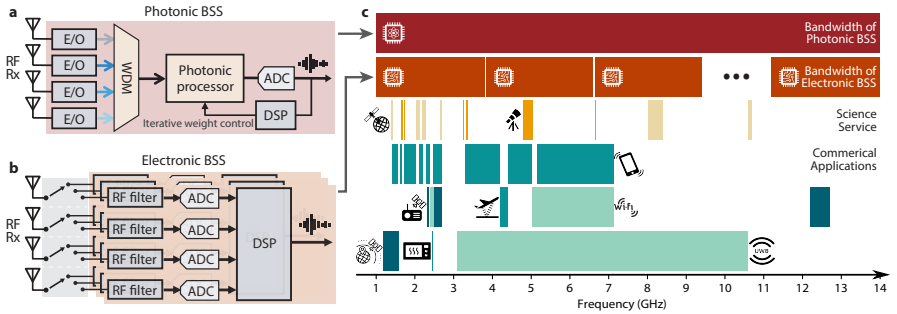


Fig. 1 Architecture comparison between electronic and photonic BSS implementation. **a**, Photonic BSS setup. **b**, Electronic BSS setup. **c**, Frequency allocation for common bands (from 1 GHz to 14 GHz) and example bandwidths for the two BSS implementations (phonics and electronics). To have the demanded bandwidth coverage usually requires a complex switching system that consists of multiple electronic BSS setups corresponding to distinct frequencies. In contrast, achieving the same coverage requires only one photonic BSS setup. Plotted Bands for science service are earth explorer satellite service (EESS) and radio astronomy service (RAS). Bands for the commercial applications are 5G cellular networks (for the first row), broadcasting-satellite service (BSS), radar altimeter, and Wi-Fi (for the second row), global positioning system (GPS), microwave oven, and ultra-wideband (UWB) (for the third row).

In this paper, we report a photonic implementation for blind source separation based on the dithering controlled MRR weightbank. Our setup fully realizes the agility of BSS by achieving a bandwidth of up to 13.8 GHz and no less than 95% separability. Compared with the previous control method, the new dithering weight control shows more than 2-bit accuracy improvement, enhancing the BSS with at least one-half reduced residual error. We also test this setup on a wireless transceiver system, proving the ability to recover a weak communication signal submerged in a wideband jamming noise, resulting in a better than 11 dB increase in signal-to-noise ratio. This work proves that the dithering controlled MRR weightbank can be an up-and-coming substitute for conventional electronic BSS, bringing about never envisioned performance in many aspects including broadband agility and higher separability.

2 Methods

BSS retrieves signals from their mixtures with minimal assumptions. If any, the signals should be statistically independent (uncorrelated) and linearly mixed. Also, the dimension of mixtures is no less than that of sources (the number of mixtures \geq the number of sources). So given the mixing matrix \mathbf{H} (full-ranked), to retain the signal of interest and eliminate the rest, the mixtures are to be weighted and summed, with weights represented by each column of the inverse matrix \mathbf{H}^{-1} . The MRR weightbank happens to be such an on-chip signal processor that can perform linear weighted addition of input signals.

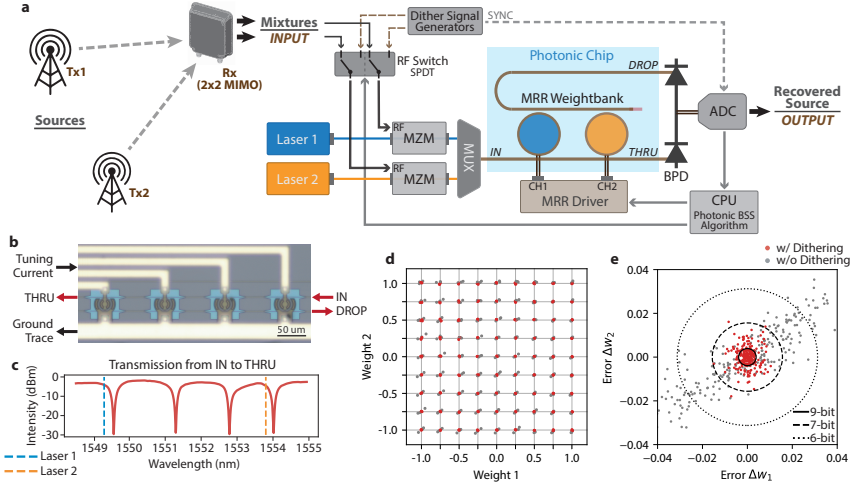


Fig. 2 Photonic BSS experimental setup. **a**, Schematic of the BSS setup. MZM, Mach-Zehnder modulator. MUX, wavelength-dependent multiplexer. BPD, balanced photodetector. ADC, analog to digital converter. Tx, transmitter. Rx, receiver. **b**, Micrograph of the MRR weightbank on the chip. **c**, Transmission spectrum of the THRU port at 25°C. **d**, Estimation of weighing accuracy. The 2-MRR weightbank in **a** was tested to tune the weights represented by each grid. The dithering control obtained the red dots, and the gray dots were obtained without the dithering. **e**, The errors of all the tested weights in **d**. A 9.0-bit of precision resulted from the dithering control and 6.7-bit for the control without the dithering.

Shown in Fig. 2a-c, the MRR weightbank consists of several round-shaped microring resonators with slightly different radii so that each has Lorentz-shaped transmission profiles (as shown in Fig. 2d) centered at different wavelengths. Each MRR is equipped with a metal heater to allow thermal tuning by varying the current applied [19]. Thus, the MRR weightbank independently weights the laser amplitudes of different wavelengths, the summation of which can be obtained by a cascaded balanced photodetector (BPD). Utilizing this ability of weighted addition, we develop a photonic BSS algorithm, which follows a pipeline consisting of three steps. Those are

the principal component analysis (PCA) [20], the whitening, and the independent component analysis (ICA) (See details in Ref. [17]). Essentially, a constrained Nelder-Mead iterative algorithm [21] is carried out that performs a projection-pursuit of the mixtures to search the optimized weighting vectors. The goal is to find the ones that the output weighted additions ($\sum w_i S_i, w_i \in [-1, 1], i \in [1, 2 \dots N], N$ is the number of the mixtures) have the maximal variance (the second-order statistic) for PCA and the maximal non-Gaussianity (the fourth-order statistic or kurtosis) for ICA.

The hardware realization of this algorithm appears as a control loop (as shown in Fig. 2a), apart from the photonic chip, also included are a BPD for e/o conversion (DSC-405, Discovery semiconductor), an ADC for signal digitization (DPO73304SX, Tektronix), a computer for statistic analysis and weight commanding, and a multi-channel current source for MRR tuning (custom-built as shown in Fig. 2d). The dithering control [18] implemented here allows driving the MRRs with less complicated drivers instead of the source-measurement unit (SMU) [16]. In this setup, the MRR driver is directly integrated into the PCB interposer, packaged close to the photonics chip with a much-reduced footprint and cable hassle [18]. The entire signal path starts from the MZM and ends at the scope, and the maximal support RF frequencies are determined by the BPD of up to 14 GHz, providing coverage for lots of commonly used RF bands. It is also worth noting that most of the signal path is of the light waveguide, bringing about broadband and flat response as well as very low latency.

The photonic chip in this setup has a 4-channel MRR weightbank ($r = 22 \mu\text{m}, \Delta r = 0.32 \mu\text{m}$) with resonance frequencies in the spacing of roughly 200 GHz. At 25 degree, the spectra of the four MRRs is shown in Fig. 2d, that the resonance peak locates at 1549.6 nm, 1551.3 nm, 1552.8 nm, and 1554.0 nm. Since this work recovers source signals from two mixtures, we use two (the leftmost and rightmost ones) among the four MRRs. The corresponding lasers (PPCL500, Pure Photonics) are tuned to be 1549.3 nm and 1553.8 nm, then amplified (FA-23, Pritel) and combined into a shared waveguide by a WDM multiplexer (MDM-15-8, Santec) before coupling into the MRR weightbank.

The implemented dithering control method [18] overcomes the low accuracy incurred by the high sensitivity. As shown in Fig. 2a, the lasers are modulated with either the actual mixtures or pre-defined dithering signals. Every time a set of commanded weights are going to be applied, the RF switch (RC-2SPDT-A18, DC - 18 GHz, Mini-Circuits) passes the dithering signals into the photonic path, which helps adjust the driving currents of the MRRs until the output weights reach the demanded values. Then, the actual mixtures are switched into the weightbank and processed. Fig. 2e illustrates the weighting accuracy, which shows the resulted weights (red dots) of the two MRRs being examined at the tested values represented by each grid point. The gray dots correspond to the resulted weights without the dithering control. An improvement of over 2 bits (from 6.7 to 9 bits) is represented by this plot, enabling the MRR weightbank to have competitive performance with its electronic counterparts.

$$\mathbf{Sep} = \frac{A_{\text{SOI}}}{\sum_i A_i} \quad (1)$$

$$\kappa(\mathbf{H}) = \|\mathbf{H}\| \cdot \|\mathbf{H}^{-1}\| \quad (2)$$

In terms of BSS, this improved weighting accuracy addresses a critical figure of merit, the separability, which describes the percentage of the signal of interest contained in a given mixture. Eq. 1 shows the calculation of the separability, which divides the amplitude of the signal of interest (A_{SOI}) by that of the summation of each signal component i in the mixture. So a higher separability means better suppression of the interference signals. Besides, reasonably estimating the BSS performance needs another figure of merit, which is the ill-condition number ($\kappa(\mathbf{H})$ defined in Eq. 2). This parameter describes the demixing difficulty calculated by the mixing matrix \mathbf{H} . Mixtures with a small ill-condition number are easier to solve. Conversely, problems with a sizeable ill-condition number are challenging and prone to smaller separability. Typically, an ill-conditioned BSS problem requires the weighting to represent the inverse matrix accurately.

To prove this, consider a simple case where the mixing matrix is symmetrical that $\mathbf{H} = [[a, 1 - a], [1 - a, a]]$, $a \in [0.5, 1]$, which is often the case that two receiver antennas and the two transmitter sources are of symmetrical positions and have identical power. Eq. 3 expresses the inverse matrix of \mathbf{H} . For maximizing the output signal amplitudes and introducing the weighting error, the actual matrix that photonic BSS applied to the mixtures can be regarded as Eq. 4, where the matrix is scaled up that the maximal output weight is reached ($w = 1$). The δ represents the weight error caused by the inaccurate MRR control.

$$\mathbf{H}^{-1} = \frac{a}{2a - 1} \begin{bmatrix} 1 & (a - 1)/a \\ (a - 1)/a & 1 \end{bmatrix} \quad (3)$$

$$\mathbf{H}'^{-1} = \begin{bmatrix} 1 + \delta & (a - 1)/a + \delta \\ (a - 1)/a + \delta & 1 + \delta \end{bmatrix} \quad (4)$$

$$\mathbf{S} = \mathbf{H}\mathbf{H}'^{-1} = \begin{bmatrix} (2a - 1)/a + \delta & \delta \\ \delta & (2a - 1)/a + \delta \end{bmatrix} \quad (5)$$

Given the Eq. 3 and Eq. 4, the coefficients (proportional to the amplitudes of each original source signal) of the separated results can be expressed by Eq. 5, by which, the percentage of error (ignore the noise) that remains in the recovered results can be regarded as $a\delta/(2a + 2a\delta - 1)$. Thus, if $a = 0.9$ given in this problem, the control accuracy improvement from 6.7 bits ($\delta \approx 0.019$) to 9 bits ($\delta \approx 0.004$) could in theory lower the error by 4.6 fold (from 2.0% to 0.44%). With this equations, we can also derive that if 2% error is permitted, this 2.3-bit improvement in control accuracy increases the solvable ill-condition number from 2.05 ($a = 0.9$) to 10 ($a = 0.55$).

In our setup, except for the demonstration on the wireless transceiver system, the signal mixtures were generated by a high-speed multi-channel

arbitrary waveform generator (N8196A, 92GSPS, Keysight) and sent to each MZM directly. We performed the generation of two baseband signals, the up-conversion and the signal mixing, all accurately through software tools (python), and then sent the mixed signals into the photonic system. This way, we have the flexibility and accuracy in controlling the carrier frequencies and the mixing matrix.

3 Results

Based on the setup described above, we examined this photonic BSS system with different problems by programming the AWG that outputs with different signal mixtures. The original two signals are repeating patterns of 16 bits, and are in format of binary phase shift keying (BPSK, bit pattern = [0, 1, 0, 1, 0, 1, 0, 1, 0, 1, 0, 1, 0, 1]) and on off keying (OOK, bit pattern = [0, 0, 1, 0, 0, 0, 1, 0, 0, 1, 0, 0, 0, 1, 0, 0]), respectively. By varying the carrier frequencies, we did BSS towards mixtures of signals of from 1 GHz to 13.8 GHz, as shown in Fig. 3. The baseband frequencies were also adjusted according to the carrier frequencies, which were 160 MHz for 1 GHz, 320 MHz for 2 - 4 GHz and 800 MHz for $f_{\text{carrier}} \geq 4.8\text{GHz}$. Annotating the two mixtures with M1 and M2 and the two original sources with S1 and S2, in this experiment, the mixing can be expressed as $M1 = 0.8 \times S1 + 0.2 \times S2$ and $M2 = 0.2 \times S1 + 0.8 \times S2$, denoting an ill-condition number of 2.26 (according to Eq. 2).

As indicated in Fig. 3, the 12 tested frequencies from 1 GHz to 13.8 GHz show no less than 95% separability. Compared with previous photonic demonstration [17], dealing with the problem of the similarly ill-condition number, we obtained almost 40 times broader bandwidth (13.8 GHz versus previously 350 MHz centered at 900 MHz) and clean signal separation across the entire band (>95% vs. previously $\approx 55\%$). This improvement in error suppression confirms the benefit of the improved dithering control method. Also, based on the FCC frequency allocation chart (partly shown in Fig. 1c), this broadband coverage by this single piece of the silicon chip ($3\text{mm} \times 8\text{mm}$) translates into the agility of processing various commonly used bands. The included bands are cellular (620 MHz - 6.425 GHz), Wi-Fi (2.4 GHz, 5 - 7.125 GHz), and those for earth explorer satellite and radio astronomy (sparsely spread from 1.4 - 10.7 GHz). This wide bandwidth can also provide full coverage to some challenging bands, such as the UWB (3.1 - 10.6 GHz).

Besides, we investigated the performance of this photonic BSS system in solving problems of different ill-condition numbers. This time, we fixed the carrier frequency at 1 GHz. And the mixing matrix is of the same symmetrical form ($\mathbf{H} = [[a, 1 - a], [1 - a, a]]$) where a was varied from 0.1 to 0.45, resulting ill-condition numbers from 2.05 to 10.1. Fig. 4 displays the separability of results obtained from setup using the improved dithering control and the previous control method (without the dithering). Noting these experimental results suffered the presence of the instrument noises, contributing to a lower separability than the theoretical values derived by Eq. 5. Albeit this noise, it

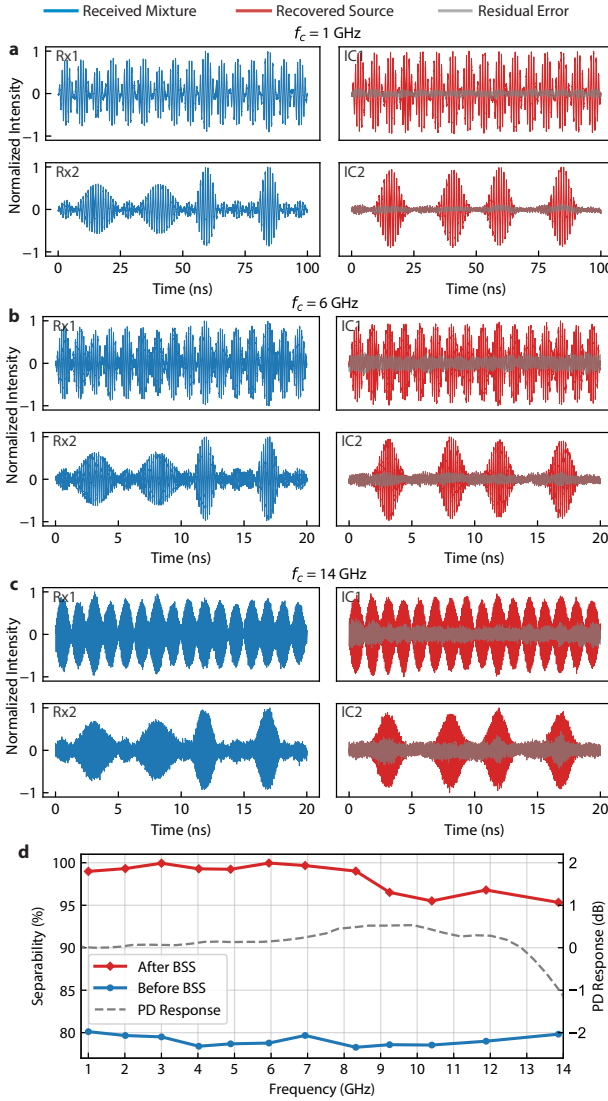


Fig. 3 Experiment result on bandwidth coverage. a-c, BSS results, the mixtures and estimated sources with carrier frequencies of 2 GHz, 4.8 GHz, and 13.8 GHz, respectively. d, The separability of the received mixtures (blue curve) and the recovered sources (red curve) versus the carrier frequency. The dashed gray curve is the relative power response of the photodetector.

generally resulted in a lower separability for a problem of a larger ill-condition number for the setup without the dithering control. Conversely, the dithering controlled setup remained a constant high separability that the influence of ill-conditioning was almost indistinguishable, being submerged by the noise. The average separability did not go lower than 96.3% for all the tested problems.

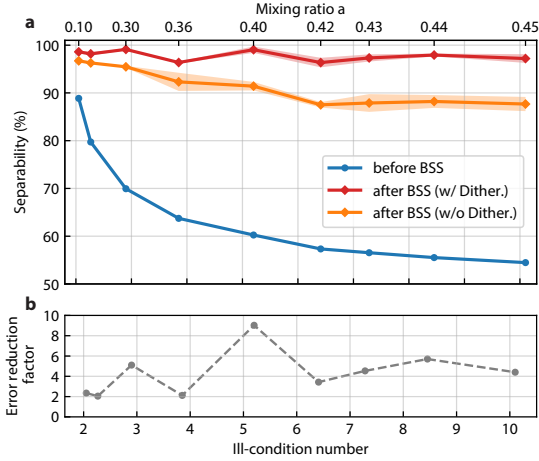


Fig. 4 BSS performance on ill-conditioned mixtures. **a**, Blue, red, and orange curves are the separability before the BSS, after BSS with dithering control, and without dithering control, respectively. The mixing matrix \mathbf{H} is defined by the mixing ratio a by $\mathbf{H} = [[a, 1 - a], [1 - a, a]]$. The corresponding ill-condition number is calculated by Eq. 2. **b**, The error reduction factor derived from **a**, which is calculated by $(1 - \text{Sep}_{w/Dither}) / (1 - \text{Sep}_{w/oDither})$.

Compared to the previous control method (the orange curve in Fig. 4), accompanied by the increased separability is the further reduction of the unwanted residuals, showing a more than two-fold decrease for all the cases and a nine-fold decrease at best (for $a = 0.40$), confirming the significance of accurate weight control for MRR-based applications like the BSS.

Next, we tested this system by solving a wireless transceiver system, which aimed to simulate the case that a communication link deteriorated by nearby RF interference. As shown in Fig. 5g, two antennas (1009-002, 1.7-2.5 GHz, Southwest Antennas) transmitted the signal of interest and a broadband jamming noise, which were mixed over the air with a transmission distance of 0.75 m. Then, the mixtures were received by a 2x2 MIMO antenna (1055-368, 1.7 - 2.5 GHz, Southwest Antennas), with two outputs corresponding to the polarization of 45-degree slant left and 45-degree slant right. The transmitted signal carried a 200-random bits sequence repeatably at a baud rate of 50 MHz. The modulation was in binary phase-shift keying (BPSK) format, and the carrier frequency is 2.1 GHz. The interference was white noise with a spectrum from 1.7 GHz to 2.5 GHz, covering the entire bandwidth of the antennas. Thus, extracting the signal of interest is insignificantly effective via spectral filtering even if the carrier frequency is known. If doable, the signal-to-noise ratio remained the same with the received mixtures at best. In contrast, the BSS can recover the communication link with no prior assumptions and suppress the interference noise. Fig. 5a-f illustrate the spectrum and the constellation diagram before and after the BSS process, where the signal-to-noise ratio has more than 11 dB improvement (16.7 dB to 27.8 dB) accompanied by a 6-fold increase of the Q value (2.16 to 12.3) from the constellation. This result

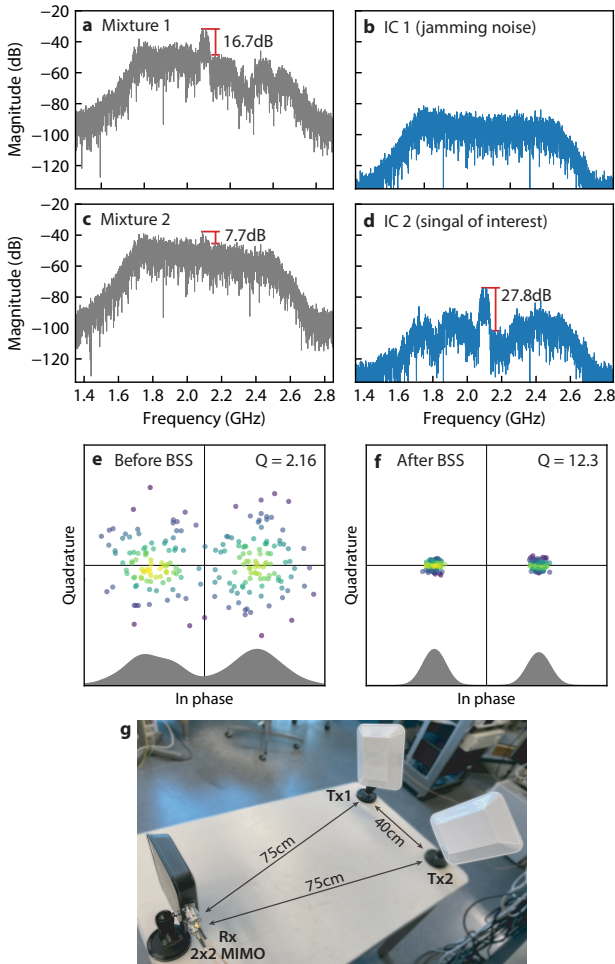


Fig. 5 BSS demonstration on wireless transceiver system. **a-b**, Spectrum of mixtures before the BSS. **c**, Spectrum of the separated jamming noise, and **d**, recovered source after BSS. Constellation diagram of **e** mixture before the BSS and **f** recovered source. **g**, Experimental setup.

demonstrated effective suppression of the nearby interference with high power and broad bandwidth, maintaining the transmission quality of the wireless communication link.

4 Conclusion

To sum up, we explored a photonic BSS approach with a much wider bandwidth of up to 13.8 GHz that could better demonstrate the potential capability of the BSS technique. Besides, the high separability revealed for all the frequencies and ill-conditioned problems, together with an example of a wireless

transceiver system, confirms that the improved MRR control method benefits the real-world applications of MRR weight banks. Overall, this work speaks that the photonic approaches are approaching the readiness to replace the conventional RF implementations, effectively addressing bandwidth limitations, energy efficiency, and latency. With the incoming availability of higher speed modulators [22] and photodetectors [23] on the silicon platform, as well the maturity of packing effort, including the photonic wire bonding [24], laser integration [25], and the co-packaging of silicon and CMOS chips, this proposed photonic BSS can have future implementations with higher integration and broader bandwidth. With these, we envision a standalone BSS device of a small form factor that is field-deployable for various applications.

Acknowledgments. This research is supported by the National Science Foundation (NSF) (ECCS-2128608 and ECCS-1642962), the Office of Naval Research (ONR) (N00014-18-1-2297 and N00014-20-1-2664), and the Defense Advanced Research Projects Agency (HR00111990049). The devices were fabricated at the Advanced Micro Foundry (AMF) in Singapore through the support of CMC Microsystems. B. J. Shastri acknowledges support from the Natural Sciences and Engineering Research Council of Canada (NSERC). S. Bilodeau acknowledges funding from the Fonds de recherche du Québec - Nature et technologies.

References

- [1] Letaief, K.B., Chen, W., Shi, Y., Zhang, J., Zhang, Y.-J.A.: The roadmap to 6g: Ai empowered wireless networks. *IEEE Communications Magazine* **57**(8), 84–90 (2019). <https://doi.org/10.1109/MCOM.2019.1900271>
- [2] Saad, W., Bennis, M., Chen, M.: A vision of 6g wireless systems: Applications, trends, technologies, and open research problems. *IEEE Network* **34**(3), 134–142 (2020). <https://doi.org/10.1109/MNET.001.1900287>
- [3] Akyildiz, I.F., Lee, W.-Y., Vuran, M.C., Mohanty, S.: Next generation/dynamic spectrum access/cognitive radio wireless networks: A survey. *Computer Networks* **50**(13), 2127–2159 (2006). <https://doi.org/10.1016/j.comnet.2006.05.001>
- [4] Larsson, E.G., Edfors, O., Tufvesson, F., Marzetta, T.L.: Massive mimo for next generation wireless systems. *IEEE Communications Magazine* **52**(2), 186–195 (2014). <https://doi.org/10.1109/MCOM.2014.6736761>
- [5] Navarro-Ortiz, J., Romero-Diaz, P., Sendra, S., Ameigeiras, P., Ramos-Munoz, J.J., Lopez-Soler, J.M.: A survey on 5g usage scenarios and traffic models. *IEEE Communications Surveys Tutorials* **22**(2), 905–929 (2020). <https://doi.org/10.1109/COMST.2020.2971781>

- [6] Venkateswaran, V., van der Veen, A.-J.: Analog beamforming in mimo communications with phase shift networks and online channel estimation. *IEEE Transactions on Signal Processing* **58**(8), 4131–4143 (2010). <https://doi.org/10.1109/TSP.2010.2048321>
- [7] Haykin, S.: Cognitive radio: brain-empowered wireless communications. *IEEE journal on selected areas in communications* **23**(2), 201–220 (2005)
- [8] Fragkiadakis, A.G., Tragos, E.Z., Askoxylakis, I.G.: A survey on security threats and detection techniques in cognitive radio networks. *IEEE Communications Surveys & Tutorials* **15**(1), 428–445 (2012)
- [9] Choi, S., Cichocki, A., Park, H.-M., Lee, S.-Y.: Blind source separation and independent component analysis: A review. *Neural Information Processing-Letters and Reviews* **6**(1), 1–57 (2005)
- [10] Yang, L., Giannakis, G.B.: Ultra-wideband communications: an idea whose time has come. *IEEE Signal Processing Magazine* **21**(6), 26–54 (2004). <https://doi.org/10.1109/MSP.2004.1359140>
- [11] Solutions, I.S.: Choosing the right rf switches for smart mobile device applications. Skyworks Solutions, Inc., Tech. Rep (2011)
- [12] Marpaung, D., Roeloffzen, C., Heideman, R., Leinse, A., Sales, S., Capmany, J.: Integrated microwave photonics. *Laser & Photonics Reviews* **7**(4), 506–538 (2013). <https://doi.org/10.1002/lpor.201200032>
- [13] Capmany, J., Mora, J., Gasulla, I., Sancho, J., Lloret, J., Sales, S.: Microwave photonic signal processing. *Journal of Lightwave Technology* **31**(4), 571–586 (2013). <https://doi.org/10.1109/JLT.2012.2222348>
- [14] Salmani, M., Eshaghi, A., Luan, E., Saha, S.: Photonic computing to accelerate data processing in wireless communications. *Opt. Express* **29**(14), 22299–22314 (2021). <https://doi.org/10.1364/OE.423747>
- [15] Tait, A.N., Wu, A.X., de Lima, T.F., Zhou, E., Shastri, B.J., Nahmias, M.A., Prucnal, P.R.: Microring weight banks. *IEEE Journal of Selected Topics in Quantum Electronics* **22**(6), 312–325 (2016). <https://doi.org/10.1109/JSTQE.2016.2573583>
- [16] Tait, A.N., Jayatileka, H., Lima, T.F.D., Ma, P.Y., Nahmias, M.A., Shastri, B.J., Shekhar, S., Chrostowski, L., Prucnal, P.R.: Feedback control for microring weight banks. *Opt. Express* **26**(20), 26422–26443 (2018). <https://doi.org/10.1364/OE.26.026422>
- [17] Ma, P.Y., Tait, A.N., Zhang, W., Karahan, E.A., de Lima, T.F., Huang, C., Shastri, B.J., Prucnal, P.R.: Blind source separation with integrated

- photonics and reduced dimensional statistics. *Opt. Lett.* **45**(23), 6494–6497 (2020). <https://doi.org/10.1364/OL.409474>
- [18] Zhang, W., Huang, C., Bilodeau, S., Jha, A., Blow, E., De Lima, T.F., Shastri, B.J., Prucnal, P.: Microring weight banks control beyond 8.5-bits accuracy. arXiv preprint arXiv:2104.01164 (2021)
- [19] Tait, A.N., de Lima, T.F., Nahmias, M.A., Shastri, B.J., Prucnal, P.R.: Multi-channel control for microring weight banks. *Opt. Express* **24**(8), 8895–8906 (2016). <https://doi.org/10.1364/OE.24.008895>
- [20] Ma, P.Y., Tait, A.N., de Lima, T.F., Abbaslou, S., Shastri, B.J., Prucnal, P.R.: Photonic principal component analysis using an on-chip microring weight bank. *Opt. Express* **27**(13), 18329–18342 (2019). <https://doi.org/10.1364/OE.27.018329>
- [21] Hyvärinen, A., Oja, E.: Independent component analysis: algorithms and applications. *Neural Networks* **13**(4), 411–430 (2000). [https://doi.org/10.1016/S0893-6080\(00\)00026-5](https://doi.org/10.1016/S0893-6080(00)00026-5)
- [22] He, M., Xu, M., Ren, Y., Jian, J., Ruan, Z., Xu, Y., Gao, S., Sun, S., Wen, X., Zhou, L., *et al.*: High-performance hybrid silicon and lithium niobate mach-zehnder modulators for 100 gbit s⁻¹ and beyond. *Nature Photonics* **13**(5), 359–364 (2019)
- [23] Lischke, S., Peczek, A., Morgan, J., Sun, K., Steckler, D., Yamamoto, Y., Korndörfer, F., Mai, C., Marschmeyer, S., Fraschke, M., *et al.*: Ultra-fast germanium photodiode with 3-db bandwidth of 265 ghz. *Nature Photonics* **15**(12), 925–931 (2021)
- [24] Lindenmann, N., Balthasar, G., Hillerkuss, D., Schmogrow, R., Jordan, M., Leuthold, J., Freude, W., Koos, C.: Photonic wire bonding: a novel concept for chip-scale interconnects. *Optics express* **20**(16), 17667–17677 (2012)
- [25] Zhou, Z., Yin, B., Michel, J.: On-chip light sources for silicon photonics. *Light: Science & Applications* **4**(11), 358–358 (2015)